JGR Oceans

RESEARCH ARTICLE
10.1029/2024JC021013

More Than Deoxygenation: Linking Iodate Reduction to Nitrogen, Iron, and Sulfur Chemistry in Reducing Regimes

Natalya Evans[1], Emma Johnson[1], Amanda Taing[1], Alexi A. Schnur[2], Peter J. Chace[3], Samantha Richards[3], Dalton S. Hardisty[2], and James W. Moffett[1]

[1]Department of Biological Sciences, University of Southern California, Los Angeles, CA, USA, [2]Department of Earth and Environmental Sciences, Michigan State University, East Lansing, MI, USA, [3]College of Earth, Ocean, and Atmospheric Sciences, Oregon State University, Corvallis, OR, USA

Key Points:

- Despite hypoxia and high Fe(II), iodide accumulation was not observed on the Oregon shelf
- Re-analysis of Oxygen Deficient Zone data reveals that most iodate depletion is not linked to oxic or nitrogenous metabolisms
- We propose iodate depletion occurs due to interaction between iodate and sulfide in sediments

Supporting Information:

Supporting Information may be found in the online version of this article.

Correspondence to:

J. W. Moffett,
jmoffett@usc.edu

Citation:

Evans, N., Johnson, E., Taing, A., Schnur, A. A., Chace, P. J., Richards, S., et al. (2024). More than deoxygenation: Linking iodate reduction to nitrogen, iron, and sulfur chemistry in reducing regimes. *Journal of Geophysical Research: Oceans*, *129*, e2024JC021013. https://doi.org/10.1029/2024JC021013

Received 6 FEB 2024
Accepted 15 SEP 2024

Author Contributions:

Conceptualization: James W. Moffett
Formal analysis: Natalya Evans, Emma Johnson, Alexi A. Schnur, James W. Moffett
Funding acquisition: James W. Moffett
Investigation: Natalya Evans, Amanda Taing, Alexi A. Schnur, Peter J. Chace, Samantha Richards, Dalton S. Hardisty, James W. Moffett
Methodology: Peter J. Chace
Project administration: James W. Moffett
Supervision: James W. Moffett
Validation: Dalton S. Hardisty
Writing – original draft: Natalya Evans
Writing – review & editing: Dalton S. Hardisty, James W. Moffett

Abstract A striking feature of Oxygen Deficient Zones (ODZs) on the eastern boundary of the Pacific Ocean are large subsurface plumes of iodide. Throughout the oceans, iodate is the predominant and thermodynamically favored species of dissolved iodine, but iodate is depleted within these plumes. The origin of iodide plumes and mechanism of reduction of iodate to iodide remains unclear but is thought to arise from a combination of in situ reduction and inputs from reducing shelf sediments. To distinguish between these sources, we investigated iodine redox speciation along the Oregon continental shelf. This upwelling system resembles ODZs but exhibits episodic hypoxia, rather than a persistently denitrifying water column. We observed elevated iodide in the benthic boundary layer overlying shelf sediments, but to a much smaller extent than within ODZs. There was no evidence of offshore plumes of iodide or increases in total dissolved iodine. Results suggest that an anaerobic water column dominated by denitrification, such as in ODZs, is required for iodate reduction. However, re-analysis of iodine redox data from previous ODZ work suggests that most iodate reduction occurs in sediments, not the water column, and is also decoupled from denitrification. The underlying differences between these regimes have yet to be resolved, but could indicate a role for reduced sulfur in iodate reduction if the sulfate reduction zone is closer to the sediment-water interface in ODZ shelf sediments than in Oregon sediments. Iodate reduction is not a simple function of oxygen depletion, which has important implications for its application as a paleoredox tracer.

Plain Language Summary Inorganic iodine has two stable forms in the ocean, iodate and iodide. In most of the subsurface ocean, iodate is the predominant compound, except in regions of the ocean without oxygen, where iodate is depleted and iodide accumulates. The causes of iodate to iodide conversion remains unclear, but it is often linked to denitrification since both iodate and nitrate can be used by anaerobic bacteria in respiration. We compared iodine behavior in the coastal margins of Oregon and Mexico's Pacific Coast. The former has no denitrification in the water column, whilst the latter has a vast subsurface zone where denitrification occurs. We sampled the low but nonzero oxygenated waters on the Oregon continental shelf. We did not observe iodide accumulation or iodate depletion, in contrast to the Mexican study area. Surprisingly, further analysis revealed that the difference is not about water column denitrification at all, but arises because processes in the shelf sediments are very different in the two regions. We now think that sulfide accumulation near the sediment water interface in Mexico but not Oregon contributes to this difference. Thus, linkage between sulfur and iodine geochemistry may determine the underlying differences between these two regimes.

1. Introduction

Iodine is a ubiquitous constituent of seawater with a nearly conservative distribution in most areas. The mean oceanic concentration of dissolved iodine is approximately 470 nM (Luther et al., 1995; Moriyasu et al., 2020), and below the thermocline, iodine is almost entirely in the form of iodate (Campos et al., 1996; Truesdale & Upstill-Goddard, 2003, and many others). The other stable form of inorganic iodine in seawater is iodide, and it accumulates in surface waters as well as oxygen deficient waters (Chance et al., 2019; Luther & Campbell, 1991; Moriyasu et al., 2020; Rue et al., 1997). Slow rates of iodide oxidation (D. S. Hardisty, Horner, Evans, et al., 2020; Luther, 2010; Luther et al., 1995; Moriyasu et al., 2023; Ştreangă et al., 2024; Wadley et al., 2020) as well as sometimes slow rates of iodate reduction (Farrenkopf et al., 1997; Hardisty, Horner, Wankel, et al., 2020) cause these oxidation state endmembers to be stable in oxic, euphotic seawater. Importantly, iodate is specifically partitioned into the carbonate mineral lattice (Hashim et al., 2022; Kerisit et al., 2018; Z. Lu et al., 2010; Podder

et al., 2017), and this fact has been used to infer past oceanic oxygen concentrations, allowing for marine iodate reconstructions throughout Earth history (Hardisty et al., 2017; Hess et al., 2023; Hoogakker et al., 2018; W. Lu et al., 2018). As such, our understanding of iodine cycling mechanisms, and specifically the conditions allowing for iodate formation and reduction, are essential for quantitative applications of carbonate-bound iodine as a paleoredox proxy tracking oxygen availability.

Extensive plumes of dissolved iodide are associated with the three major oxygen deficient zones (ODZs) in the world's oceans. These regions are characterized by extremely low oxygen concentrations (<10 nM) such that nitrate replaces oxygen as the primary terminal electron acceptor (Zakem & Follows, 2017), Thermodynamically, iodate reduction is more favorable than nitrate reduction in these regions, and the main metabolic reactions of these regions are nitrate-reducing. There have been several theories coupling iodate reduction to denitrifying processes, such as iodate reduction as a byproduct of nitrate-reducing enzymes (Amachi et al., 2007; Farrenkopf et al., 1997) as well as iodate being coupled with nitrite by chemoautotrophs (Babbin et al., 2017). In addition, a facultative anaerobe that reduces iodate chemoheterotrophically has been identified (Reyes-Umana et al., 2021), and proteins similar to those possessed by this organism, capable of iodate reduction, have been found within an ODZ (Saunders et al., 2022). Hydrogen sulfide can reduce iodate rapidly through abiotic reactions (Jia-Zhong & Whitfield, 1986). While sulfide is commonly observed in reducing shelf sediments, it is rarely observed in ODZs.

The accumulation of iodide within ODZs is associated with a decrease in iodate. However, dissolved iodide accumulation is typically far in excess of the iodate loss, indicating an external source increasing the total dissolved inorganic iodine concentration beyond 470 nM (Cutter et al., 2018; A. M. Farrenkopf & Luther, 2002; Moriyasu et al., 2020). This excess iodine originates from reducing shelf sediments, where dissimilatory sulfate reduction produces sulfide, which liberates iodide from organically bound iodide. Nearby bottom waters with excess iodide concentrations are transported into the ODZs (Evans et al., 2020; Moriyasu et al., 2020; Scholz et al., 2024). Reducing shelf sediments were identified as the source of this iodide because the ratio of iodine to carbon in marine organic matter is $\sim 10^{-4}$ (Elderfield & Truesdale, 1980; Wong & Brewer, 1977), which is far lower than the amount required to produce this excess iodide signal from remineralization of sinking particles (Cutter et al., 2018; Farrenkopf & Luther, 2002).

In this manuscript, we report dissolved iodine speciation from a hypoxic, Eastern Boundary Upwelling System continental shelf to examine the processes that cause iodate depletion. Our continental shelf data comes from Oregon, which experiences seasonal hypoxia (O_2 < 60 μM) (Adams et al., 2013). Summer hypoxia is known to produce extremely high Fe(II) concentrations in bottom waters (Evans et al., 2023; Lohan & Bruland, 2008), suggesting that this continental shelf can become extremely reducing (Siedlecki et al., 2015). Oregon continental shelf waters typically remain hypoxic, though occasional sulfidic events have occurred (Chan et al., 2008). We compare our findings from Oregon against re-processed data from the Eastern Tropical North Pacific (ETNP) ODZ that leverages the extensive analysis of its iodine distribution (Moriyasu et al., 2020), iodate reduction rates (D. S. Hardisty, Horner, Evans, et al., 2020), and hydrographic features (Evans et al., 2020). Water masses were found to have a significant role on the iodate distribution (D. S. Hardisty, Horner, Evans, et al., 2020), and we apply a new water mass analysis technique to the region to identify the mechanisms causing iodate depletion.

2. Materials and Methods

2.1. Sampling Description

Oregon continental margin samples were collected on the R/V *Oceanus* during the OC2107A cruise from July to August 2021 as well as the OC2111A cruise during November 2021. We sampled during summer hypoxia in OC2107A, whereas OC2111A had bottom water oxygen concentrations closer to 100 μM. The sampling locations for these two cruises are presented in Figure 1. Samples were collected from a Seabird CTD equipped with 10 or 12 L GO-FLO bottles and a SBE43 sensor for measuring oxygen concentrations. Samples were filtered using 0.45 μm Corning disposable bottle top filters within 3 hours of collection and then frozen for analysis on land. For OC2107A, this manuscript focuses primarily on stations 31–33, which were collected on the Heceta Bank. This region serves as a hotspot for deoxygenation (Siedlecki et al., 2015) and benthic iron fluxes because it is a semi-retentive shelf (Gan & Allen, 2005) fed organic matter from the Umpqua River (Severmann et al., 2010). These samples were collected at least 110 km north of the North Hydrate Ridge, a location with extremely high porewater iodine (Z. Lu et al., 2008).

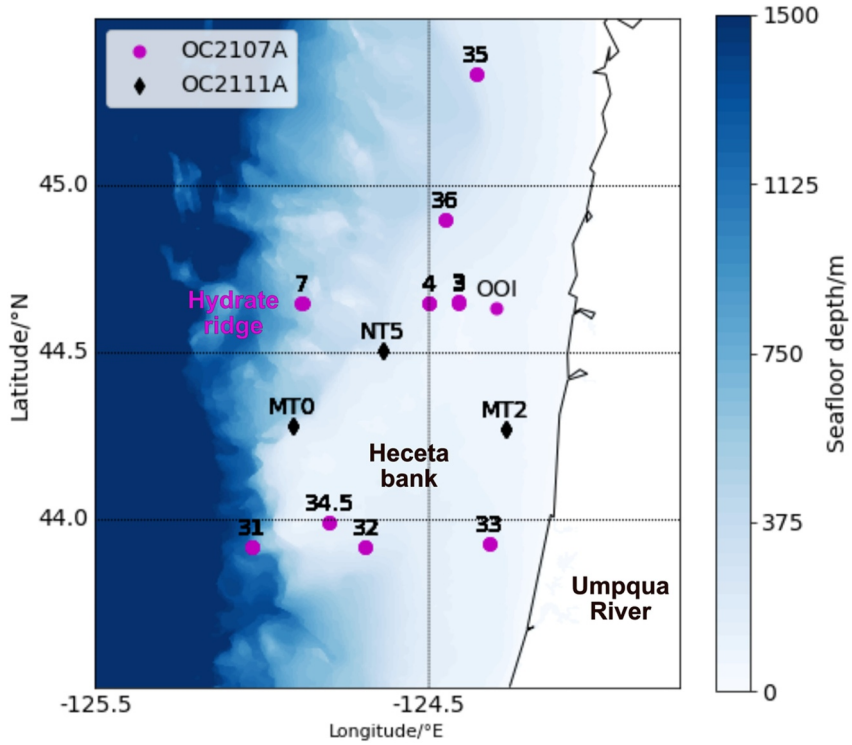

Figure 1. Map of stations on the Oregon coast during OC2107A and OC2111A cruises overlaid on seafloor depth. The location of the Endurance array, discussed in this manuscript, is labeled as OOI, and other regions of interest, such as the Heceta Bank, the Umpqua River, and the Hydrate ridge are also labeled.

During OC2111A, we also collected iodine samples using a benthic boundary gradient sampler at stations MT0 and MT2. This lander held five 1 L GO-FLO bottles mounted at known heights. Samples were collected simultaneously via a burn wire that fired after the lander sat on the seafloor for 30 min. For these samples, oxygen concentrations were measured less than an hour from recovery using a Presens TX-3 micro optode in a flow cell fitted to the sampling syringe outlets. Between each O_2 measurement, brief flushes of nitrogen gas were also used to check for calibration shifts and remove contamination between samples. Iron(II) was also measured following the methods described in Evans et al. (2023) for these lander samples. These near-bottom samples had high Fe(II), which lowers the potential risk of contamination. We measured Fe(II) to compare their benthic profiles, since both of these compounds have the same reducing shelf source. Figure 1 depicts sampling locations.

2.2. Chemical Analyses

Iodide was quantified with cathodic square wave stripping voltammetry using either a calomel or an Ag/AgCl reference electrode (Rue et al., 1997), adapted from Luther et al. (1988). The BioAnalytical Systems (BASi) Controlled Growth Mercury Electrode was set to the Static Mercury Drop setting and interfaced with a BASi Epsilon ε2 voltammetric analyzer. Each 10 mL seawater sample was measured in duplicate by treatment with 150 μL of 0.2% Triton X 100 (Sigma Aldrich—BioX grade) and purging with argon for five minutes to avoid oxygen interference (Tian & Nicolas, 1995). Previous studies have found that argon is required for removing dissolved oxygen, as nitrogen was insufficient (Moriyasu et al., 2023). Scans used a drop size of 7, deposition time of 30 s, and 5 s of quiet time. Scan increments were set to be 2 mV with a scan range between −140 and −700 mV, and the square wave amplitude and frequency were 25 mV and 125 Hz. Each sample was measured in duplicate and their signals were averaged. Calibration was performed using standard additions of potassium iodide to a seawater sample. This standard addition was performed using a GEOTRACES GP15 sample with less than 20 nM iodide as the sample matrix and increasing 20 nM increments were added to fresh splits from that GP15 sample until 120 nM had been added. These adaptations to the calibration protocol were required to measure the extremely low iodide concentrations in the Oregon samples.

Iodate was not directly measured for the Oregon samples. As we were primarily interested in the amount of dissolved iodine released from the continental margin, we measured the total dissolved iodine using a similar method to Hardisty, Horner, Wankel, et al. (2020) at Michigan State University (MSU). This method can measure total iodine as the sum of dissolved iodide, dissolved iodate, and dissolved organic iodine in addition to measuring the individual species separately. Total iodine was measured by reducing these iodine species to iodide by acidification with hydrochloric acid (Fisher; pH not monitored) followed by immediate addition of sodium bisulfite (Fisher) for a final concentration of 0.6 mM then letting the samples sit overnight (Hou et al., 2001). Iodide was extracted from the seawater samples by running the samples through AG1-X8 resin then eluting with 15 mL of 2.0 M nitric acid (Fisher) and 18% tetramethylammonium hydroxide (TMAH, Fisher). We note that this method was optimized for isotope tracer measurements via sparge-based MC-ICP-MS but, while it can also quantify concentrations, that other approaches may be preferred for large transects requiring high sample throughput (e.g., IC UV/VIS (Jones et al., 2023)). In addition, while TMAH is commonly used to stabilize iodine, it is a category 1 central nervous system toxin and thus other bases may be preferred if feasible (e.g., ammonium hydroxide (Winkelbauer et al., 2021)). Once iodide was eluted in 2.0 M nitric acid and 18% TMAH, these solutions were diluted to 1/40th of this concentration and quantified on a Thermo-Fisher iCAP TQ Inductively Coupled Plasma-Mass Spectrometer (ICP-MS) using internal standards of cesium, indium, and rhodium (Inorganic Ventures) at 5–10 ppb, which targets 150–800k cps. The ICP-MS was tuned before each set of measurements using Thermo-Fisher iCAP TQ tuning solution (Fisher) and calibrated for iodide using eight standards diluted from a stock iodide solution (Inorganic Ventures). In addition, a recovery sample with a known concentration was processed through the analytical train to estimate sample recovery. 40 samples were measured for total dissolved iodine, and of these, nine samples had anomalously low total dissolved iodine with less than 400 nM (mostly >373 nM, but one sample as low as 333 nM). We also extracted iodide to measure on the ICP-MS at MSU, which allowed us to inter-compare this method with the hanging mercury drop electrode method. For this protocol, we did not reduce the samples before adding them to our columns. Instead, we added untreated seawater to the AG1-X8 resin columns to retain the iodide then eluted the iodate and organic iodine fractions using milliQ water and 0.2 M potassium nitrate rinses, then eluted the iodide with the same 15 mL of 2.0 M nitric acid and 18% TMAH solution. Due to the low concentrations of iodide, we measured these solutions with a 1/20th dilution rather than a 1/40th dilution on the ICP-MS, otherwise, this analytical chain was identical to the total iodine measurements.

Our monitored yields for standards are within the typical range (Hardisty, Horner, Wankel, et al., 2020) and independent measurements of iodide (the iodine species total iodine is analyzed as) via IC-ICPMS and Hg electrode show good correlation. That said, we are cautious to interpret these low values given the potential for low yields from the chromatographic procedure (e.g., Hou et al., 2007). In addition, Cook et al. (2022) outline potential impacts of acidification of samples on iodine speciation, which could be used to optimize the pre-column sample treatment for total iodine. Since we did not confirm total iodine measurements via the sum of independent measurements of iodide, iodate, and DOI, we note that, unlike our iodine intercomparison, the total iodine measurements do not serve as an intercomparison. Given the above, we maintain these total iodine data in Table S2 in Supporting Information S1, but have filtered them from plots in the main text.

2.3. Computational Methods

Water mass analysis via the pyompa package was performed in Google Colaboratory using the scripts provided in https://github.com/NatalyaEvans/Iodine_Frontiers. After performing water mass analysis, the results were plotted and processed using MATLAB R2018B (The MathWorks Inc, 2018) and visualized using perceptually uniform colormaps (Thyng et al., 2016). TEOS-10 calculations (McDougall & Barker, 2011) were performed in MATLAB as well with the IBM ILOG CPLEX Optimization Studio V12.8.0 as an optimizer. Linear regression comparing the measured and simulated iodate was performed using the "lsqfitma" command in MATLAB (Glover et al., 2011).

Maps were plotted using Python 3.7.13 (Python Software Foundation, 2022) in Spyder 5.1.5 (Raybaut, 2009) with the Basemap package (Hunter, 2007). Bathymetry data were downloaded from the National Centers for Environmental Information 3 arc-second resolution coastal relief model (https://www.ngdc.noaa.gov/mgg/coastal/crm.html). The fraction of ODZ conditions presented in Figures 2a and 4a depicts how consistently certain locations are found to be oxygen deficient using an atlas of oxygen deficient conditions (Kwiecinski & Babbin, 2021).

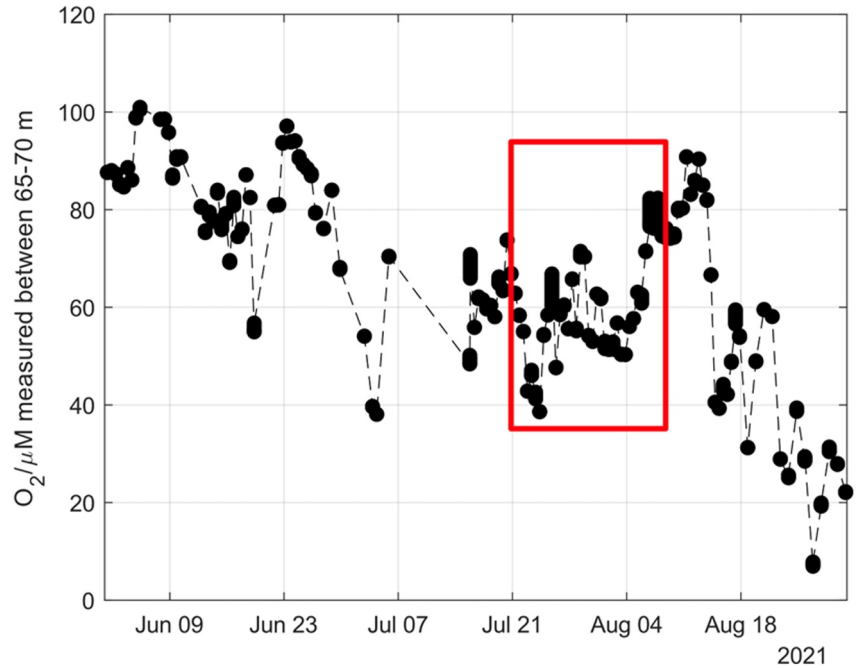

Figure 2. Subsurface oxygen concentrations during the summer of 2021 from the Endurance array, with the period where we sampled during OC2107A annotated using a red box.

3. Results

3.1. Summer Conditions on the Oregon Shelf

It is important to assess conditions at our study site in the period prior to the cruise. If hypoxia began just before our summer cruise, it could be possible that not enough time passed for iodate depletion to be obvious. We did not have the chance to collect oxygen measurements year-round, but the Oregon Shelf Surface Piercing Profiler Mooring in the Endurance array (https://oceanobservatories.org/site/ce02shsp/) measures subsurface oxygen concentrations continuously using an Aanderaa—Optode 4831. This mooring traverses up and down the water column at 44.6372°N, 124.299°W, with a seafloor depth of 81 m. This mooring infrequently measures oxygen below 70 m, so we chose to analyze the oxygen concentrations between 10 and 15 m from the seafloor. This time series reveals that the oxygen concentrations we observed during OC2107A appear to have persisted for approximately a month (Figure 2).

3.2. Distribution of Redox-Active Compounds During Summer

During our summer cruise in Oregon continental margin waters, we sampled consistently hypoxic bottom waters on the Heceta Bank. This region is known for more intense hypoxia (Siedlecki et al., 2015) and higher benthic iron fluxes (Severmann et al., 2010) than its surroundings. When we sampled there, the oxygen concentrations on shelf bottom waters (stations 33–32) were 28–50 μM and the oxygen concentration on the continental slope bottom water (station 31) was 8 μM. Despite the fact that these bottom waters were hypoxic rather than anoxic, we observed extremely high concentrations of Fe(II), between 40 and 47 nM (Figure 3). These results indicate that even though the water column is hypoxic, high amounts of organic carbon in the sediment cause porewaters to become strongly anoxic near the sediment-water interface.

We observe minimal iodide accumulation on the Heceta Bank (Figure 4d). The highest iodide concentration is a surface sample measured off-shelf, though there is one bottom water sample with 72 nM iodide. These values are more similar to limited, or lack thereof, iodide in offshore ODZ regions, such as the North Pacific (Moriyasu et al., 2023) but are far lower than nearshore anoxic regions such as Pacific ODZs, with 400–800 nM iodide and far lower Fe(II) concentrations (Cutter et al., 2018; Moriyasu et al., 2020). We also observed a middepth iodide feature on our most coastal Heceta Bank station, and we attribute this middepth feature to iodide flux from lateral

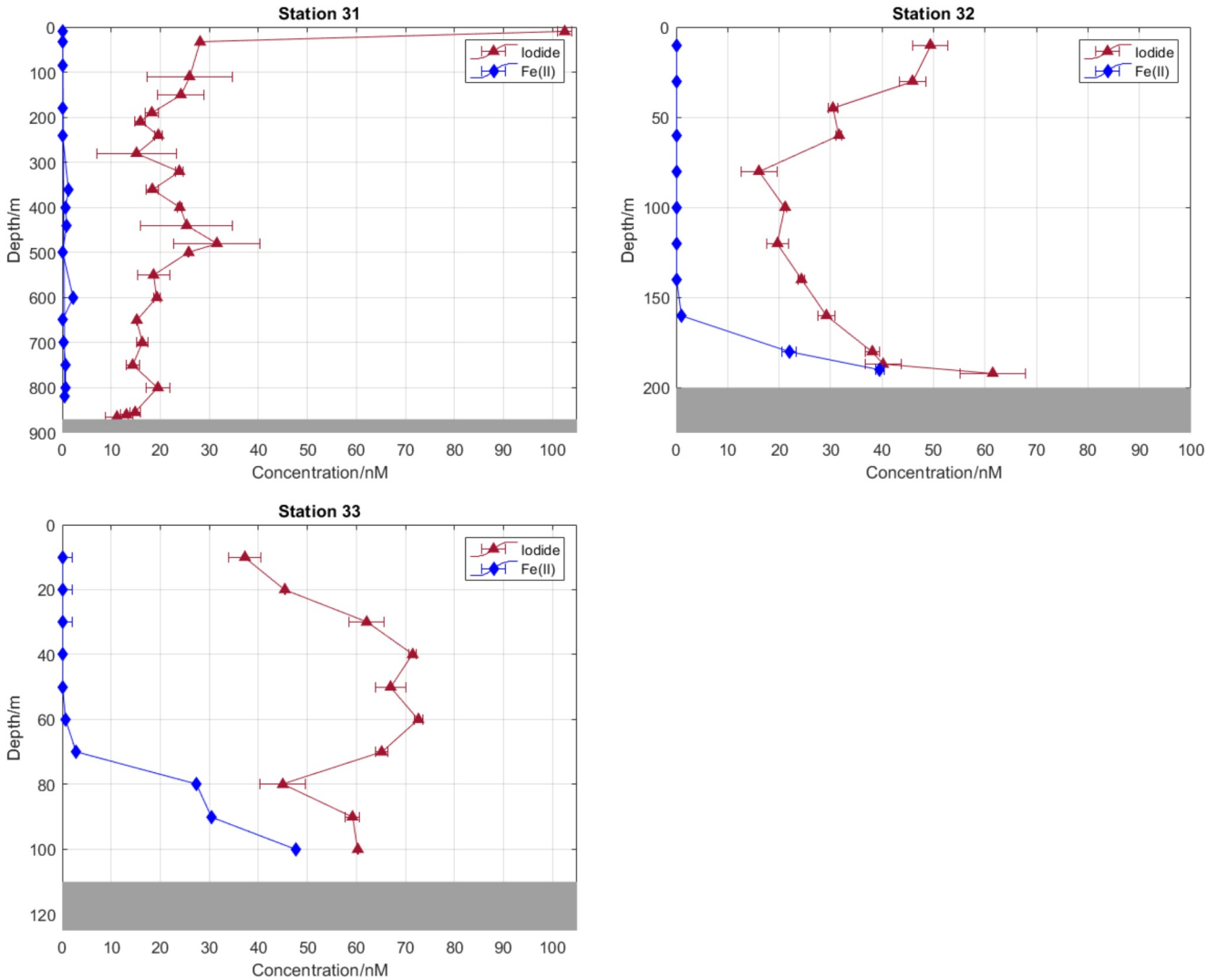

Figure 3. Water column profiles of iodide and Fe(II) for station 31–33 of OC2107A on the Oregon coast. The gray region on the bottom represents the seafloor depth.

advection away from a shallower benthic source, or potentially the Umpqua River. Total dissolved iodine (Figure 4c) shares this middepth feature at the most coastal station, suggesting that this iodide flux corresponds with a flux of total iodine. The mid-Heceta Bank station where iodide accumulates to 72 nM has 478 nM total dissolved iodine, whereas other samples at this station have 420–485 nM total dissolved iodine.

3.3. Distribution of Redox-Active Compounds During Winter

Hypoxia in Oregon is typical in summer, with much higher oxygen concentrations during the winter. We were interested in exploring how these oxic conditions contrasted with our summer observations, and as such collected iodine data during OC2111A in November 2021. We provide water column profiles of oxygen and iodide at stations MT2 and MT0, with seafloor depths of 198 and 259 m, appropriately (Figure 5). At MT2, both oxygen and iodide decrease almost linearly from the surface. In the bottom-most sample of MT2, the iodide concentration actually increases to 47 nM, suggesting a sediment source of iodide that does not mix into the rest of the water column.

We also deployed a benthic boundary gradient sampler at these two stations on the northern Heceta Bank in November 2021, with results presented in Figure 6. Unfortunately, this expedition occurred in the winter and therefore we did not sample hypoxic waters, even in the benthic boundary layer. Nevertheless, we observed both

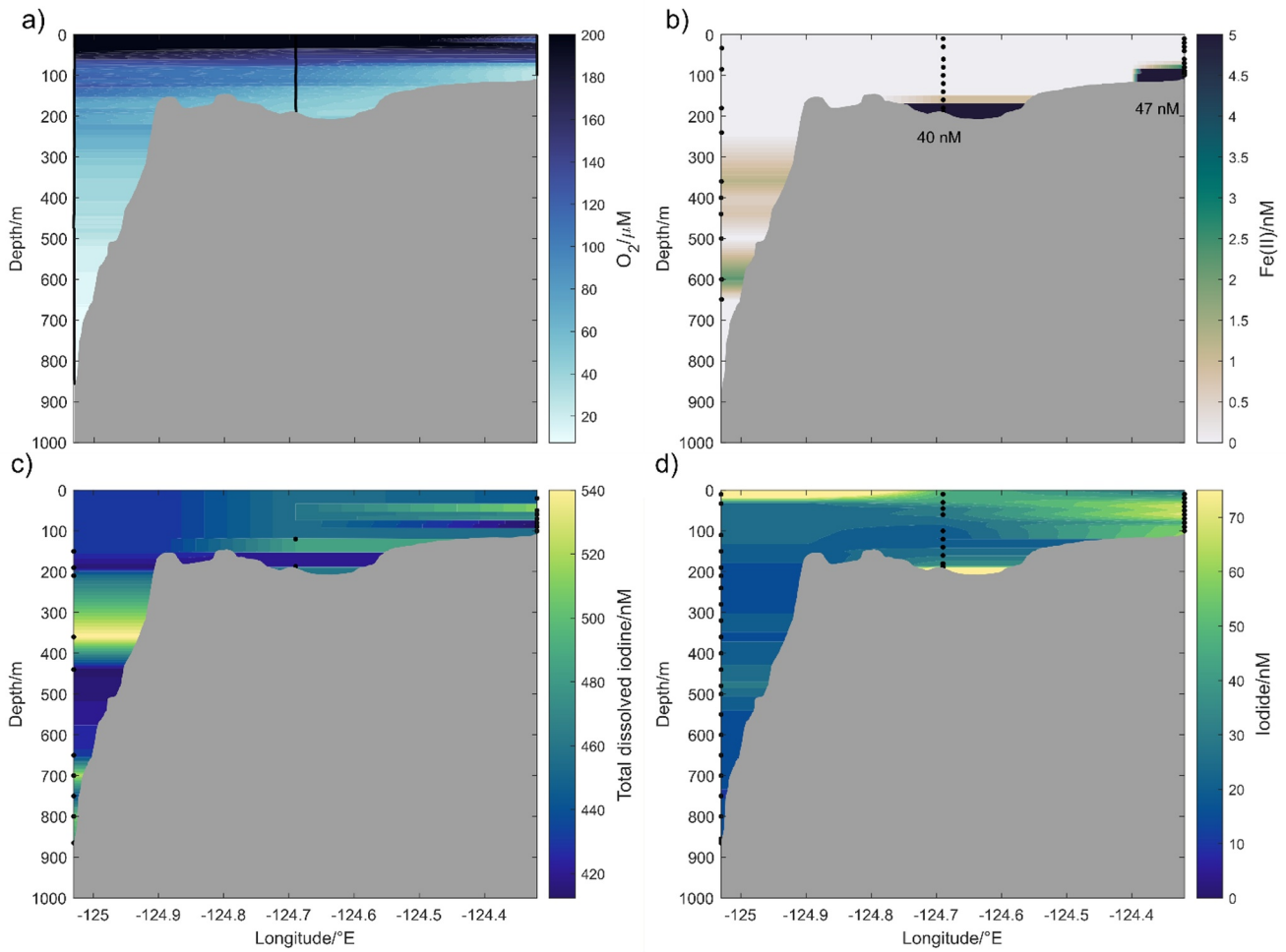

Figure 4. Distribution of (a) oxygen, (b) Fe(II), (c) total dissolved iodine, and (d) iodide measured on the Heceta Bank on OC2107A in summer. Total dissolved iodine here is measured as the sum of iodate, iodide, and dissolved organic iodide. The gray background represents the bathymetry of Heceta Bank, whereas black points represent sampling depths. Sections were filled by first interpolating each station linearly every 1 m vertically, then interpolating across longitude linearly.

Fe(II) and iodide in these samples, despite the 80–90 μM of oxygen. While oxygen depletion is clearly observed closer to the seafloor, trends in iodide and Fe(II) are far less coherent. At MT2, none of the benthic boundary layer profiles have the same trend. At MT0, iodide and Fe(II) do have similar profiles, though neither match the oxygen profile. In addition, the profiles for iodide and Fe(II) appear to decrease closer to the seafloor. These differences in profile shape likely emerge due to different cross-shelf transport at these locations. These velocity data are presented in Figure S8 in Supporting Information S1.

These benthic lander data reveal high correlations between iodide and total dissolved iodine concentrations ($r = 0.875$). These results suggest that the continental margin is acting as a source of iodine to the water column. This conclusion was difficult to acquire from water column profiles alone, likely due to the influence of river iodine and increased mixing in the water column, and these two factors are less significant for the benthic boundary gradient profiles.

4. Discussion

4.1. Analysis of Oregon Data

The iodine/calcium proxy is commonly used to reconstruct oxygen concentrations in the geologic past because iodate depletion occurs in anoxic waters. However, iodide concentrations only reach 72 nM on the Oregon shelf and approximately 19 nM off-shelf, compared to the approximate 470 nM concentration of total dissolved

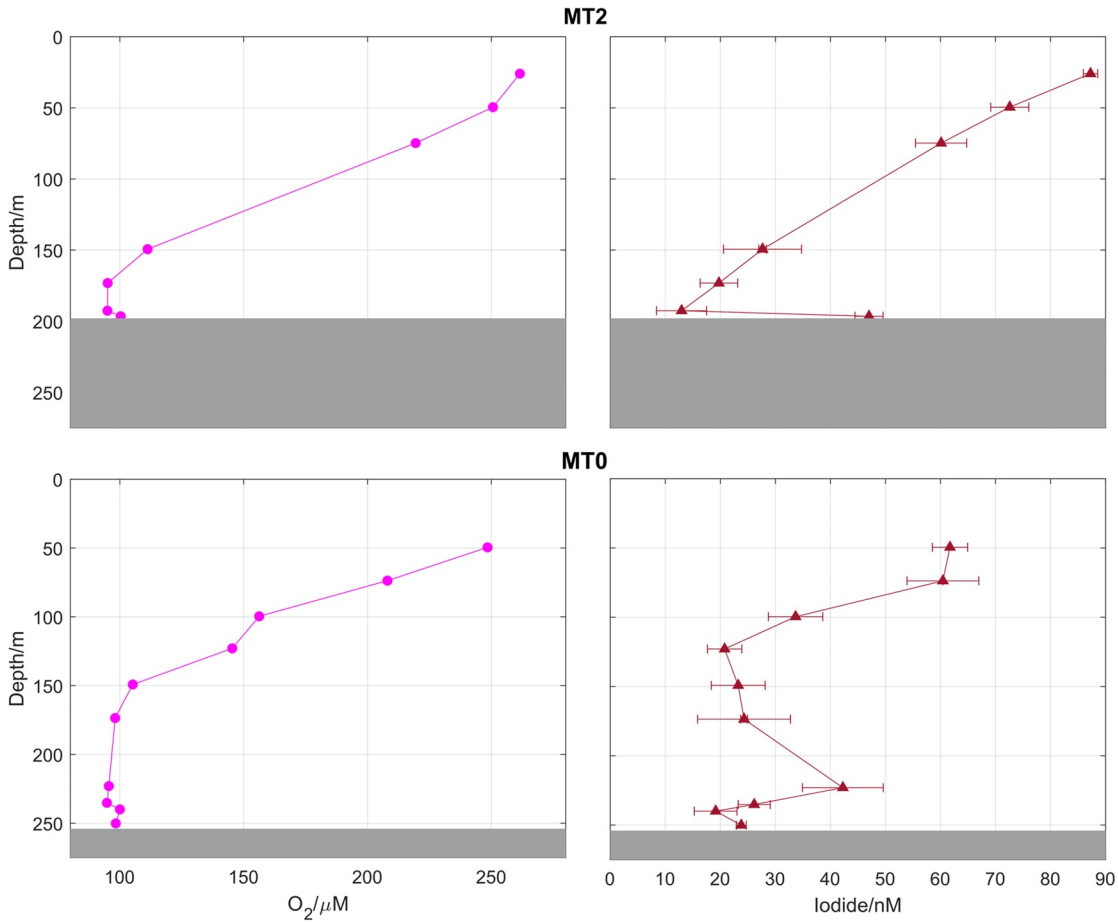

Figure 5. Water column profiles of oxygen and iodide, measured via hanging mercury drop electrode, for the MT2 and MT0 stations of OC2111A. The gray region on the bottom of each plot represents the seafloor depth.

inorganic iodine, whereas Fe(II) accumulates as high as 47 nM on-shelf and 2 nM off-shelf on the hypoxic (8 μM) Oregon continental margin compared to their far lower concentrations in ODZs, typically below 1 nM (Bolster et al., 2022). These results reveal that neither iodate depletion nor iodide accumulation are generally correlated with bottom water oxygen nor reducing strength, assessed via Fe(II) accumulation. In select regions like ODZs, iodate depletion and Fe(II) accumulation are linked (Cutter et al., 2018), which allows iodide to be implemented as a non-oxidizing tracer for shelf-derived Fe. Nevertheless, the results from our comparison suggest that linkages between the iodine cycle and oxygen concentrations, as well as the iodine cycle and Fe(II) concentrations, may be regionally specific rather than broadly applicable. Given these observations, we examine multiple factors below that may be responsible for water column iodate depletion.

Winter benthic boundary layer data reveal the sediments' contribution to iodine measured in the water column. However, the bottom water profile of MT0 during OC2111A depicts a decreasing value near the sediment-water interface. While counterintuitive at first, these data profiles can be explained from the near-bottom velocities measured by the lander during sample collection. We propose that since MT0 was collected on the continental slope, these benthic profiles sampled material during coherent off-shelf transport, whereas on the continental shelf, MT2 experienced less coherent advection and therefore this profile reflects material from a wider range of source locations on the shelf. The water column profiles of iodide and oxygen corresponding to these benthic boundary layer deployments are presented in Figure 6, It is also interesting to note that we observe 20–40 nM increases in iodide and total dissolved iodine despite approximately 90 μM oxygen concentrations. Nevertheless, the Fe(II) measured in these benthic lander data accumulates to higher concentrations than in the ETNP ODZ, so reductive dissolution must still be occurring in the continental shelf sediments. In addition, this Oregon Fe(II) accumulation leads to nearly a tenth less iodide accumulation than in the ETNP ODZ, where iodide

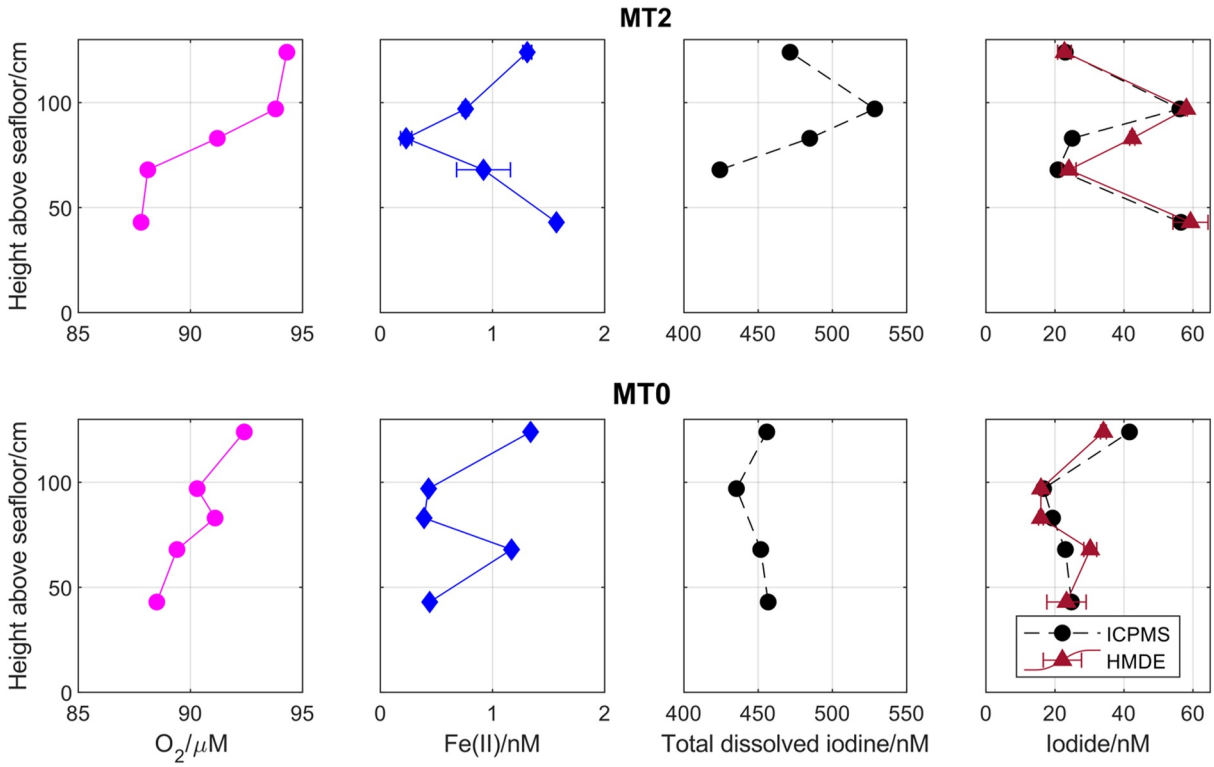

Figure 6. Profiles collected from a benthic boundary gradient lander at stations MT2 (top) and MT0 (bottom). Iodide samples measured with a hanging mercury drop electrode are labeled "HMDE" whereas samples measured with an ICPMS are labeled "ICPMS."

concentrations easily reach 470 nM. The entire iodide data set is plotted against oxygen in Figure S9 in Supporting Information S1. There is little correlation across all stations, reflecting iodide persistence in the presence of oxygen and the production of iodide by phytoplankton in the euphotic zone.

4.2. Re-Analysis of ETNP ODZ Data

Water masses provide a framework for analyzing the causes of spatial variability as well as identifying processes related to respiration. Evans et al. (2020) found that the 13°C Water (13CW), Northern Equatorial Pacific Intermediate Water, and Antarctic Intermediate Water (AAIW) were the primary water masses that compose the Eastern Tropical North Pacific ODZ (ETNP ODZ). Additional information about these water masses can be found in Evans et al. (2020) and references therein. Evans et al. (2020) deconvoluted ETNP ODZ samples into their source waters, but this deconvolution relied on local nutrient concentrations for their water mass definitions and therefore could not calculate respiration. With this source water deconvolution, Hardisty, Horner, Wankel, et al. (2020) indicated that water mass mixing contributed to but did not exclusively control the iodate distribution of the ETNP ODZ. Unfortunately, these previous analyses did not fully describe respiration within the ETNP ODZ, and therefore could not fully identify the factors influencing the iodate distribution.

Advances in optimum multiparameter analysis has resulted in a method for quantifying the amount of aerobic versus anaerobic respiration in ODZs (Evans et al., 2023). We applied this methodology to the FK180624 iodine data from the ETNP ODZ (Moriyasu et al., 2020), using a similar analysis as performed in Hardisty, Horner, Wankel, et al. (2020). In Hardisty, Horner, Wankel, et al. (2020), the iodate concentration was estimated as a function of only water mass mixing (Equation 1), whereas the method applied in this paper includes two respiration pathways (Equation 2). These respiration pathways are differentiated using their observed stoichiometries in the ETNP ODZ, given in Equations 3 and 4, where n_1 ranges from 14 to 17 μmol kg^{-1} and n_2 ranges from −65 to −40 μmol kg^{-1}. After calculating the water mass contents and extent of respiration pathways, we used these parameters as predictor variables in a multi-linear regression. This approach enables calculation of the equivalents of iodate changed per unit of phosphate released by these two metabolisms, as differentiated via

Table 1
Deconvolution Results for Simulating the Iodate Distribution in the Eastern Tropical North Pacific Oxygen Deficient Zone

Name	Endmember concentration or stoichiometry ratio	Standard error
13CW	103 nM	28 nM
NEPIW	479 nM	25 nM
AAIW	413 nM	26 nM
Aerobic respiration	116 nM IO_3^-/μM PO_4^{3-}	54 nM IO_3^-/μM PO_4^{3-}
Anaerobic respiration	−1,750 nM IO_3^-/μM PO_4^{3-}	200 nM IO_3^-/μM PO_4^{3-}

nitrate stoichiometry. Simultaneously, we also calculate the endmember concentrations of iodate in each water mass. In Equations 1 and 2, the "a_{1-3}" coefficients represent the endmember concentration of iodate in each water mass, and the "x" coefficients represent the fraction of each water mass. The advancements in this paper enable deconvolution due to the amount of respiration that has occurred, which is represented by xi (ξ) symbols. The a_4 and a_5 coefficients represent the ratio of iodate changed per phosphate for each metabolism. More information about this method is included in the supplemental information.

$$\left[IO_3^-\right] = a_1 x_{13CW} + a_2 x_{NEPIW} + a_3 x_{AAIW} \quad (1)$$

$$\left[IO_3^-\right] = a_1 x_{13CW} + a_2 x_{NEPIW} + a_3 x_{AAIW} + a_4 \xi_{aerobic} + a_5 \xi_{anaerobic} \quad (2)$$

$$(CH_2O)_{106}(NH_3)_{16}(PO_4) + O_2 \rightarrow\ 106\ CO_2 + n_1\ NO_3 + PO_4 \quad (3)$$

$$(CH_2O)_{106}(NH_3)_{16}(PO_4) + n_2\ NO_3 \rightarrow\ 106\ CO_2 + \frac{n_2 + 16}{2}\ N_2 + PO_4 \quad (4)$$

Our iodate deconvolution (Table 1) reveals that one water mass, the 13°C Water (13CW) has an endmember concentration of only 100 ± 30 nM iodate when sampled on this transect. Since this water mass has a mean transit time of approximately 50 years before entering the ETNP ODZ (Margolskee et al., 2019), it likely has time for its iodate endmember concentration to reach ~475 nM, the mean subsurface concentration in this region, Therefore, the 375 nM iodate deficit in this water mass must occur within the ETNP ODZ. This water mass enters the ETNP ODZ on its southeast boundary, and is advected by the West Mexican Coastal Current into the northern ODZ (Gómez-Valdivia et al., 2015) along continental shelf sediments (Evans et al., 2020), where it was sampled on FK180624. Since this iodate deficit is reported in the 13CW endmember, rather than being lumped into anaerobic respiration, suggested that a mechanism besides net nitrate-removing metabolisms is responsible for most iodate depletion in the ETNP ODZ. The median iodate concentration removed by anaerobic respiration is 143 nM, which is approximately a third of the iodate removed by other mechanisms in the 13CW.

4.3. Potential Mechanisms Causing Iodate Depletion

The data from the Oregon hypoxic zones show little or no iodate depletion, even when conditions are sufficiently reducing for Fe(II) to accumulate (Evans et al., 2024). This finding is significant because thermodynamically, iodate and Fe(II) should not coexist. Previously, we have argued that Fe(II) in the water column of the Oregon shelf arises from benthic sources. One would therefore expect a substantial flux of iodide accompanying the Fe (II), but these fluxes are small, relative to ODZ systems. These observations suggest that the Oregon and ODZ systems are quite distinct, even though benthic Fe(II) fluxes are a characteristic of both. Therefore, a comparative approach has been used throughout this study to identify the key differences.

The water mass deconvolution reveals that anaerobic respiration, or a correlated process, contributes to the observed iodate depletion in the ETNP ODZ. However, the deconvolution revealed that most of the iodate depletion observed in the ETNP ODZ occurred through a process that primarily affects the 13°C water mass (13CW) but is not linked to denitrification.

The transport of the 13CW along continental margin sediments means that this water mass has been significantly exposed to processes that occur near and in sediments before reaching the northern ODZ. Processes known to reduce iodate, which we might expect to encounter at the benthic-water column interface, include dissimilatory

nitrate reduction (Amachi et al., 2007; Farrenkopf et al., 1997), chemoheterotrophic reduction (Reyes-Umana et al., 2021), and reduction via abiotic oxidation of sulfide (Jia-Zhong & Whitfield, 1986). Microbial nitrite oxidation by iodate has also been proposed by Babbin et al. (2017) as a chemoautotrophic process. Our deconvolution shows that dissimilatory nitrate reduction does not explain the 13CW iodate deficit and is not the cause of iodate depletion.

Nitrite is an intermediate in denitrification, therefore nitrite re-oxidation is likely to be important in the water column near zones with active denitrification (Babbin et al., 2017), provided a suitable oxidant is available. However, denitrification and nitrite re-oxidation in the water column have distinctly different stoichiometries that hinders our water mass deconvolution from delineating nitrite re-oxidation from anaerobic respiration quantitatively. Despite this uncertainty, the observed nitrite re-oxidation in the ETNP ODZ is implicitly included within our water mass analysis via the stoichiometry of denitrification used, so it is highly unlikely that it generates the magnitude of iodate reduction that we observe in the ETNP ODZ (Babbin et al., 2020; Beman et al., 2013; Peng et al., 2015).

It is important to consider how these considerations apply to Oregon. Since nitrite re-oxidation is rare in denitrifying sediments and there is no active denitrification and hence nitrite accumulation in the hypoxic water column on the Oregon shelf, nitrite re-oxidation is not likely to be a sink for iodate in the water column or sediments there.

4.4. Likelihood of Sulfide Accumulation Causing Iodate Reduction

The aforementioned considerations lead us to the conclusion that most iodate depletion observed in the ETNP ODZ arises from the shelf, with reduction by sulfide being the most plausible possibility that we have not already ruled out. The redox reaction between sulfide and iodate is rapid (Jia-Zhong & Whitfield, 1986); far faster than sulfide and oxygen (Luther, 2010; Luther et al., 2011). Plumes of sulfide have periodically emerged in the ETSP ODZ (Schunck et al., 2013), but this phenomenon has not yet been observed in the ETNP ODZ. Sulfide production does occur within reducing microenvironments in large sinking particles in the ETNP ODZ (Raven et al., 2020), but this is a relatively small source of sulfide to the water column. While the waters of the ETNP ODZ remain nitrogenous, the maximum sulfate reduction rate appears less than 2 cm below the sediment-water interface. These lines of evidence suggest that abiotic reduction of iodate to iodide via reacting with sulfide in sediments of the ETNP continental shelf as the most plausible explanation for the observed iodate depletion in the ETNP ODZ.

The reducing sediments off the Oregon coast might be expected to be another strong source of iodide to the water column, resulting in significant plumes, yet they are not. Differences in shelf biogeochemistry regarding iron and sulfur speciation and their links to iodine cycling might account for this difference. Sediments near the Oregon shelf do not reach their maximum sulfate reduction rates until 5 cm below the sediment-water interface, whereas ETNP sediments on the Mexican continental shelf reach their maximum sulfate reduction rates shallower than 5 cm (Kristensen et al., 1999). Data from Kristensen et al. (1999) are replotted in Figure 7 for illustration. This difference in the depth of the maximum measured sulfate reduction rate relative to the sediment-water interface suggests that porewater sulfide is more likely to reach bottom waters and reduce iodate in the ETNP ODZ, as seen in Figure 7. The high concentrations of iron in Oregon likely hinders sulfide reaching the bottom waters, preventing iodate depletion.

Beyond the ETNP, sulfide accumulation may explain why iodate depletion was observed in hypoxic waters in the Benguela Upwelling System (Truesdale & Bailey, 2000) but not Oregon waters. The Benguela Upwelling System is known for sulfidic bottom waters (Brüchert et al., 2003; Lavik et al., 2009; Ohde & Dadou, 2018) and the strong hypoxia observed by Truesdale and Bailey (2000) could have caused sulfidic sediment conditions, which would lower iodate concentrations. These factors all increase the confidence that sulfide accumulation, especially near the sediment-water interface in reducing shelf sediments (Figure 7), serves as one of the primary drivers of iodate depletion in the water column.

Table 2 summarizes the processes we hypothesize cause iodate depletion and the lines of evidence supporting or eliminating them. The primary driver of iodate depletion must explain the iodate depletion in the 13CW, but cannot correlate with anaerobic respiration in the ETNP, and does not occur in Oregon shelf waters. While chemoautotrophic coupling to nitrite re-oxidation seems plausible, this reaction rarely occurs in reducing

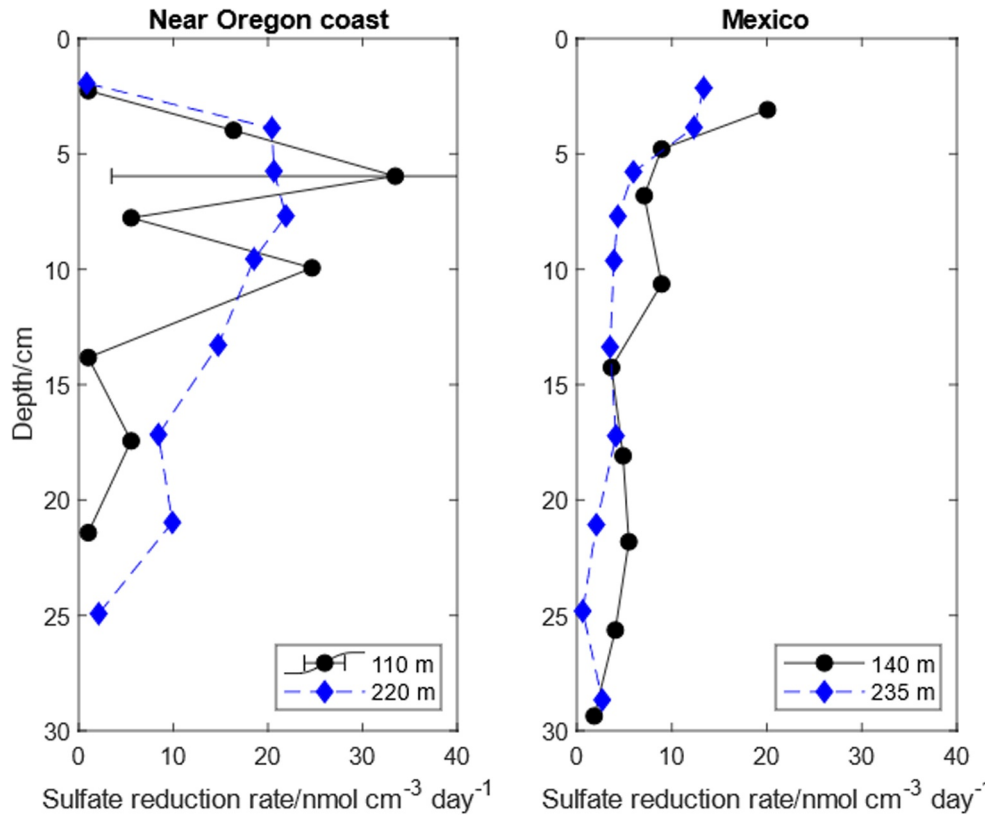

Figure 7. Sulfate reduction rates measured in sediments on the Washington continental shelf, by Oregon, as well as the Mexican continental shelf below the Oxygen Deficient Zone, replotted from data reported in Kristensen et al. (1999).

sediments and therefore cannot supply the excess iodine signal that we observed in the ETNP. This fact suggests that abiotic reduction with sulfide is most likely, although chemoheterotrophic reduction remains a possibility.

4.5. Other Mechanisms for Iodate Reduction

We should consider other mechanisms for iodate reduction as well. Fe(II) is the predominant form of dissolved Fe in the anaerobic water column of the ETNP ODZ, and in the benthic boundary layer of the winter Oregon continental shelf. We also note that dissolved Fe is thermodynamically favorable and has been observed as a reductant of iodate to iodide (Councell et al., 1997; Jiang et al., 2023; Luther, 2023). Councell et al. (1997) observed up to 98% reduction of iodate to iodide within hours in solutions with 20:1 and 10:1 Fe:IO_3. The Fe:IO_3 ratios are lower on the Oregon shelf with a maximum of 1:2 which is a range that Councell et al. (1997) did not test. These lower ratios could imply that Fe is limiting for iodate reduction but could still account for at least some

Table 2
Summary of Iodate Depletion Mechanisms and Whether They Agree or Not With Observations of Iodate Depletion

Mechanism	Correlates with anerobic resp. in the ETNP?	Explains 13CW iodate deficit?	Occurs in or near Oregon shelf waters
Low substrate affinity dissimilatory nitrate reduction	Yes, high confidence	No, high confidence	Yes, high confidence
Chemoautotrophic coupling to nitrite oxidation	Maybe, low confidence	No, medium confidence	No, high confidence
Chemoheterotrophic reduction at sub-μM O_2	Maybe, low confidence	Maybe, low confidence	Maybe, low confidence
Abiotic reduction with sulfide	No, high confidence	Yes, high confidence	No, medium confidence
Abiotic reduction with Fe	No, high confidence	No, high confidence	Maybe, low confidence
Observational data	No	Yes	No

portion of the maximum iodide values near 70 nM. Nevertheless, while not measured in this study, Severmann et al. (2010) demonstrated benthic Fe values as high as 2 μM in the same region and porewater values well in excess of 2 μM. This distribution is somewhat analogous to that of sulfide, which reaches mM values commonly in pore fluids, but benthic and water column plume values are typically in the low μM range. In either case, both benthic Fe and sulfide have the potential to be non-limiting for iodate reduction.

We must also consider different rates of iodide oxidation in these regimes. Iodide is thermodynamically unstable in the water column overlying the Oregon shelf, since oxygen is always present. While iodide oxidation cannot explain the absence of excess iodine, which is based on the total inventory of both redox states, it could contribute to the low overall fraction of iodide observed in all of our Oregon samples. The mechanism is unknown, but it has been linked to ammonia oxidizing bacteria in cultures and in a global model (Wadley et al., 2020). Estimates of iodide oxidation rates reported in Moriyasu et al. 2023) are consistent with the results of that model. Reactive oxygen species produced by the oxidation of Fe(II) by molecular oxygen, specifically the OH radical, might also oxidize iodide (Luther, 2023). Sustained ROS production was directly observed via Fe oxidation of sulfide in the presence of O_2 within hydrothermal plumes (Shaw et al., 2021). While this mechanism of iodate production along the Oregon shelf is currently speculative, it also cannot be ruled out. Future studies could perform iodine incubations targeting these redox reactions to provide constraints on the mechanisms driving both iodine oxidation and reduction.

4.6. Implications for the I/Ca Proxy

These lines of evidence suggest that abiotic reduction with sulfide may be an important source of iodate depletion. We suggest that low iodate concentrations, and hence low I/Ca ratios, may specifically indicate low oxygen water masses which have interacted with either water column or sedimentary sulfide. Iodate depletion clearly occurs in regions with sulfidic water columns (Luther & Campbell, 1991; Wong & Brewer, 1977), and thus this proxy would be effective in these conditions. The lack of iodate depletion on the Fe-rich Oregon continental shelf indicates that the I/Ca proxy decouples from oxygen in Fe-rich, reducing regions. This finding includes the caveat that O_2 was present, albeit low, on the Oregon shelf. Therefore, it cannot be ruled out that chemoheterotrophic iodate reduction may require O_2 thresholds lower than currently recognized (sub-μM) or, alternatively, that OH radicals oxidize iodide to iodate in environments with high dissolved Fe and present oxygen.

The I/Ca proxy is highly reliable in modern ODZs because of sulfidic porewaters near the sediment-water interface, but what about water columns that are denitrifying but lack nearby sulfidic sediments? These systems could still have iodate depletion due to chemoautotrophic nitrite oxidation, however, the relative magnitude of this process versus sulfide oxidation on iodate depletion is unknown. Regions that have denitrifying water columns but lack sulfidic porewaters near sediment-water interfaces are rare. Fortunately, the incomplete denitrification in the Bay of Bengal implies that high amounts of nitrite re-oxidation occur there (D'Asaro et al., 2020).

If sulfidic environments, whether in the water column or near/at the sediment-water interface, are important for iodate depletion within a water mass, there may be important implications for the interpretation of I/Ca ratios through Earth history. Specifically, the degree of widespread ferruginous versus euxinic bottom water conditions may play a currently underappreciated role in regulating iodate availability through time, as opposed to exclusively O_2 concentrations. In this model, I/Ca ratios may be relatively higher in time periods with elevated marine oxygen as well as when oxygen is low, but ferruginous conditions are more widespread relative to euxinic conditions. In the latter scenario, elevated iodate is produced in settings with sufficient O_2 but persists in these low O_2, ferruginous environments. While this hypothesis requires additional confirmation, it could have implications for increases in I/Ca in the Proterozoic and early Paleozoic, when ferruginous conditions were more widespread (Hardisty et al., 2017; Lu et al., 2018; Sperling et al., 2015).

5. Conclusions

The most important conclusion of the study is that whilst there are benthic sources of iodide in both the Oregon and ETNP systems, only in the ETNP does it result in (a) near-complete depletion of iodate in much of the water column and (b) accumulation of excess iodine in the form of iodide. Comparison with other studies suggests that these conclusions can be generalized to other margin systems. Excess iodine and iodate depletion are characteristic of ODZs, while absent in eastern boundary upwelling regimes lacking water column denitrification like off the African Coast (Hughes et al., 2021). These observations suggest that water column processes, rather than

benthic processes, determine iodine redox speciation. Yet our deconvolution results point clearly to a margin-based reduction mechanism for iodate that is decoupled from dissimilatory nitrogen reduction. We argue that reduction by sulfide within sediments is the most plausible explanation, while recognizing that such a mechanism should be important in reducing sediments even when the overlying water column is aerobic. It is possible that reduction by sulfide leads to larger iodide fluxes in ODZs because the sulfide boundary is much closer to the sediment-water interface, due to the iron reduction present in Oregon sediments. As such, the magnitude of iodate reduction is not directly linked to redox processes in the anaerobic water column of the ODZ, but is dependent on the availability of sulfide to the sediment-water interface. Our work suggests the potential that iodate may persist, even under relatively low oxygen, which has implications for the use of iodate as a paleoredox tracer for reconstruction of ancient marine oxygen availability. Future work should focus on determining the mechanisms driving iodate reduction in coastal upwelling settings to provide more quantitative understanding of the drivers of spatiotemporal iodate variations in modern and ancient marine settings.

Data Availability Statement

Data for this paper has been uploaded to BCO-DMO (https://www.bco-dmo.org/project/889751) Moffett (2024). Code for making figures, performing water mass analysis, and processing the water mass analysis data to identify iodate processes are available at https://zenodo.org/doi/10.5281/zenodo.13742820 (Evans, 2024).

Acknowledgments

We would like to acknowledge NSF OCE #2023708 for funding research on the Oregon shelf. DH acknowledges funding from NSF-OCE #1923218. The development of the benthic sampler lander was supported by Oregon Sea Grant Project number: R/HBT-23-Reimers2022 with the syringe sampler (Susane) graciously provided from Ifremer. The authors declare no conflicts of interest. We appreciate the support provided by R/V *Oceanus* crew and marine technicians during our cruise, specifically Emily Shimada, Michael Tepper-Rasmussen, and Sabrina Taraboletti.

References

Adams, K. A., Barth, J. A., & Chan, F. (2013). Temporal variability of near-bottom dissolved oxygen during upwelling off central Oregon. *Journal of Geophysical Research: Oceans*, *118*(10), 4839–4854. https://doi.org/10.1002/jgrc.20361

Amachi, S., Kawaguchi, N., Muramatsu, Y., Tsuchiya, S., Watanabe, Y., Shinoyama, H., & Fujii, T. (2007). Dissimilatory iodate reduction by marine *Pseudomonas* sp. strain SCT. *Applied and Environmental Microbiology*, *73*(18), 5725–5730. https://doi.org/10.1128/AEM.00241-07

Babbin, A. R., Buchwald, C., Morel, F. M. M., Wankel, S. D., & Ward, B. B. (2020). Nitrite oxidation exceeds reduction and fixed nitrogen loss in anoxic Pacific waters. *Marine Chemistry*, *224*, 103814. https://doi.org/10.1016/j.marchem.2020.103814

Babbin, A. R., Peters, B. D., Mordy, C. W., Widner, B., Casciotti, K. L., & Ward, B. B. (2017). Multiple metabolisms constrain the anaerobic nitrite budget in the Eastern Tropical South Pacific: Nitrogen Dynamics in the Eastern Tropical South Pacific. *Global Biogeochemical Cycles*, *31*(2), 258–271. https://doi.org/10.1002/2016GB005407

Beman, J. M., Leilei Shih, J., & Popp, B. N. (2013). Nitrite oxidation in the upper water column and oxygen minimum zone of the eastern tropical North Pacific Ocean. *The ISME Journal*, *7*(11), 2192–2205. https://doi.org/10.1038/ismej.2013.96

Bolster, K. M., Heller, M. I., Mulholland, M. R., & Moffett, J. W. (2022). Iron and manganese accumulation within the Eastern Tropical North Pacific oxygen deficient zone. *Geochimica et Cosmochimica Acta*, *334*, 259–272. https://doi.org/10.1016/j.gca.2022.07.013

Brüchert, V., Jørgensen, B. B., Neumann, K., Riechmann, D., Schlösser, M., & Schulz, H. (2003). Regulation of bacterial sulfate reduction and hydrogen sulfide fluxes in the central namibian coastal upwelling zone. *Geochimica et Cosmochimica Acta*, *67*(23), 4505–4518. https://doi.org/10.1016/S0016-7037(03)00275-8

Campos, M. L. A. M., Farrenkopf, A. M., Jickells, T. D., & Luther, G. W. (1996). A comparison of dissolved iodine cycling at the Bermuda Atlantic Time-series Station and Hawaii Ocean Time-series Station. *Deep Sea Research Part II: Topical Studies in Oceanography*, *43*(2), 455–466. https://doi.org/10.1016/0967-0645(95)00100-X

Chan, F., Barth, J. A., Lubchenco, J., Kirincich, A., Weeks, H., Peterson, W. T., & Menge, B. A. (2008). Emergence of Anoxia in the California Current Large Marine Ecosystem. *Science*, *319*(5865), 920. https://doi.org/10.1126/science.1149016

Chance, R. J., Tinel, L., Sherwen, T., Baker, A. R., Bell, T., Brindle, J., et al. (2019). Global sea-surface iodide observations, 1967–2018. *Scientific Data*, *6*(1), 286. https://doi.org/10.1038/s41597-019-0288-y

Cook, M. K., Dial, A. R., & Hendy, I. L. (2022). Iodine stability as a function of pH and its implications for simultaneous multi-element ICP-MS analysis of marine carbonates for paleoenvironmental reconstructions. *Marine Chemistry*, *104148*, 104148. https://doi.org/10.1016/j.marchem.2022.104148

Councell, T. B., Landa, E. R., & Lovley, D. R. (1997). Microbial reduction of iodate. *Water, Air, and Soil Pollution*, *100*(1), 99–106. https://doi.org/10.1023/A:1018370423790

Cutter, G. A., Moffett, J. W., Nielsdóttir, M. C., & Sanial, V. (2018). Multiple oxidation state trace elements in suboxic waters off Peru: In situ redox processes and advective/diffusive horizontal transport. *Marine Chemistry*, *201*, 77–89. https://doi.org/10.1016/j.marchem.2018.01.003

D'Asaro, E., Altabet, M., Kumar, N. S., & Ravichandran, M. (2020). Structure of the Bay of Bengal oxygen deficient zone. *Deep Sea Research Part II: Topical Studies in Oceanography*, *179*, 104650. https://doi.org/10.1016/j.dsr2.2019.104650

Elderfield, H., & Truesdale, V. W. (1980). On the biophilic nature of iodine in seawater. *Earth and Planetary Science Letters*, *50*(1), 105–114. https://doi.org/10.1016/0012-821X(80)90122-3

Evans, N. (2024). [software]. https://doi.org/10.5281/zenodo.13742820

Evans, N., Boles, E., Kwiecinski, J. V., Mullen, S., Wolf, M., Devol, A. H., et al. (2020). The role of water masses in shaping the distribution of redox active compounds in the Eastern Tropical North Pacific oxygen deficient zone and influencing low oxygen concentrations in the eastern Pacific Ocean. *Limnology & Oceanography*, *65*(8), 1688–1705. https://doi.org/10.1002/lno.11412

Evans, N., Floback, A. E., Gaffney, J., Chace, P. J., Luna, Z., Knoery, J., et al. (2024). The role of seasonal hypoxia and benthic boundary layer exchange on iron redox cycling on the Oregon shelf. *Limnology & Oceanography*, *69*(4), 742–756. https://doi.org/10.1002/lno.12476

Evans, N., Tichota, J., Moffett, J. W., & Devol, A. H. (2023). Prolific nitrite reoxidation across the Eastern Tropical North Pacific Ocean. *Limnology & Oceanography*, *68*(8), 1719–1733. https://doi.org/10.1002/lno.12380

Farrenkopf, A. M., Dollhopf, M. E., Chadhain, S. N., Luther, G. W., & Nealson, K. H. (1997). Reduction of iodate in seawater during Arabian Sea shipboard incubations and in laboratory cultures of the marine bacterium Shewanella putrefaciens strain MR-4. *Marine Chemistry*, *57*(3), 347–354. https://doi.org/10.1016/S0304-4203(97)00039-X

Farrenkopf, A. M., & Luther, G. W. (2002). Iodine chemistry reflects productivity and denitrification in the Arabian Sea: Evidence for flux of dissolved species from sediments of western India into the OMZ. *Deep Sea Research Part II: Topical Studies in Oceanography*, *49*(12), 2303–2318. https://doi.org/10.1016/S0967-0645(02)00038-3

Gan, J., & Allen, J. S. (2005). Modeling upwelling circulation off the Oregon coast. *Journal of Geophysical Research*, *110*(C10). https://doi.org/10.1029/2004JC002692

Glover, D. M., Jenkins, W. J., & Doney, S. C. (2011). *Modeling methods for marine science*. Cambridge University Press.

Gómez-Valdivia, F., Parés-Sierra, A., & Flores-Morales, A. L. (2015). The Mexican Coastal Current: A subsurface seasonal bridge that connects the tropical and subtropical Northeastern Pacific. *Continental Shelf Research*, *110*, 100–107. https://doi.org/10.1016/j.csr.2015.10.010

Hardisty, D. S., Horner, T. J., Evans, N., Moriyasu, R., Babbin, A. R., Wankel, S. D., et al. (2020). Limited iodate reduction in shipboard seawater incubations from the Eastern Tropical North Pacific oxygen deficient zone. *Earth and Planetary Science Letters*, *554*, 116676. https://doi.org/10.1016/j.epsl.2020.116676

Hardisty, D. S., Horner, T. J., Wankel, S. D., Blusztajn, J., & Nielsen, S. G. (2020). Experimental observations of marine iodide oxidation using a novel sparge-interface MC-ICP-MS technique. *Chemical Geology*, *532*, 119360. https://doi.org/10.1016/j.chemgeo.2019.119360

Hardisty, D. S., Lu, Z., Bekker, A., Diamond, C. W., Gill, B. C., Jiang, G., et al. (2017). Perspectives on Proterozoic surface ocean redox from iodine contents in ancient and recent carbonate. *Earth and Planetary Science Letters*, *463*, 159–170. https://doi.org/10.1016/j.epsl.2017.01.032

Hashim, M. S., Burke, J. E., Hardisty, D. S., & Kaczmarek, S. E. (2022). Iodine incorporation into dolomite: Experimental constraints and implications for the iodine redox proxy and Proterozoic Ocean. *Geochimica et Cosmochimica Acta*, *338*, 365–381. https://doi.org/10.1016/j.gca.2022.10.027

Hess, A. V., Auderset, A., Rosenthal, Y., Miller, K. G., Zhou, X., Sigman, D. M., & Martínez-García, A. (2023). A well-oxygenated eastern tropical Pacific during the warm Miocene. *Nature*, *619*(7970), 521–525. https://doi.org/10.1038/s41586-023-06104-6

Hoogakker, B. A. A., Lu, Z., Umling, N., Jones, L., Zhou, X., Rickaby, R. E. M., et al. (2018). Glacial expansion of oxygen-depleted seawater in the eastern tropical Pacific. *Nature*, *562*(7727), 410–413. https://doi.org/10.1038/s41586-018-0589-x

Hou, X., Aldahan, A., Nielsen, S. P., Possnert, G., Nies, H., & Hedfors, J. (2007). Speciation of 129I and 127I in seawater and implications for sources and transport pathways in the North sea. *Environmental Science & Technology*, *41*(17), 5993–5999. https://doi.org/10.1021/es070575x

Hou, X., Dahlgaard, H., & Nielsen, S. P. (2001). Chemical speciation analysis of 129I in seawater and a preliminary investigation to use it as a tracer for geochemical cycle study of stable iodine. *Marine Chemistry*, *74*(2), 145–155. https://doi.org/10.1016/S0304-4203(01)00010-X

Hughes, C., Barton, E., Hepach, H., Chance, R., Pickering, M. D., Hogg, K., et al. (2021). Oxidation of iodide to iodate by cultures of marine ammonia-oxidising bacteria. *Marine Chemistry*, *234*, 104000. https://doi.org/10.1016/j.marchem.2021.104000

Hunter, J. D. (2007). Matplotlib: A 2D graphics environment. *Computing in Science & Engineering*, *9*(3), 90–95. https://doi.org/10.1109/MCSE.2007.55

Jiang, Z., Cui, M., Qian, L., Jiang, Y., Shi, L., Dong, Y., et al. (2023). Abiotic and biotic reduction of iodate driven by Shewanella oneidensis MR-1. *Environmental Science & Technology*, *57*(48), 19817–19826. https://doi.org/10.1021/acs.est.3c06490

Jia-Zhong, Z., & Whitfield, M. (1986). Kinetics of inorganic redox reactions in seawater: I. The reduction of iodate by bisulphide. *Marine Chemistry*, *19*(2), 121–137. https://doi.org/10.1016/0304-4203(86)90044-7

Jones, M. R., Chance, R., Dadic, R., Hannula, H.-R., May, R., Ward, M., & Carpenter, L. J. (2023). Environmental iodine speciation quantification in seawater and snow using ion exchange chromatography and UV spectrophotometric detection. *Analytica Chimica Acta*, *1239*, 340700. https://doi.org/10.1016/j.aca.2022.340700

Kerisit, S. N., Smith, F. N., Saslow, S. A., Hoover, M. E., Lawter, A. R., & Qafoku, N. P. (2018). Incorporation modes of iodate in calcite. *Environmental Science & Technology*, *52*(10), 5902–5910. https://doi.org/10.1021/acs.est.8b00339

Kristensen, E., Devol, A. H., & Hartnett, H. E. (1999). Organic matter diagenesis in sediments on the continental shelf and slope of the Eastern Tropical and temperate North Pacific. *Continental Shelf Research*, *19*(10), 1331–1351. https://doi.org/10.1016/S0278-4343(99)00024-2

Kwiecinski, J. V., & Babbin, A. R. (2021). A high-resolution atlas of the eastern tropical Pacific oxygen deficient zones. *Global Biogeochemical Cycles*, *35*(12), e2021GB007001. https://doi.org/10.1029/2021GB007001

Lavik, G., Stührmann, T., Brüchert, V., Van der Plas, A., Mohrholz, V., Lam, P., et al. (2009). Detoxification of sulphidic African shelf waters by blooming chemolithotrophs. *Nature*, *457*(7229), 581–584. https://doi.org/10.1038/nature07588

Lohan, M. C., & Bruland, K. W. (2008). Elevated Fe(II) and dissolved Fe in hypoxic shelf waters off Oregon and Washington: An enhanced source of iron to coastal upwelling regimes. *Environmental Science & Technology*, *42*(17), 6462–6468. https://doi.org/10.1021/es800144j

Lu, W., Ridgwell, A., Thomas, E., Hardisty, D. S., Luo, G., Algeo, T. J., et al. (2018). Late inception of a resiliently oxygenated upper ocean. *Science*, *361*(6398), eaar5372. https://doi.org/10.1126/science.aar5372

Lu, Z., Jenkyns, H. C., & Rickaby, R. E. M. (2010). Iodine to calcium ratios in marine carbonate as a paleo-redox proxy during oceanic anoxic events. *Geology*, *38*(12), 1107–1110. https://doi.org/10.1130/G31145.1

Lu, Z., Tomaru, H., & Fehn, U. (2008). Iodine ages of pore waters at Hydrate Ridge (ODP Leg 204), Cascadia Margin: Implications for sources of methane in gas hydrates. *Earth and Planetary Science Letters*, *267*(3), 654–665. https://doi.org/10.1016/j.epsl.2007.12.015

Luther, G. W. (2010). The role of one- and two-electron transfer reactions in forming thermodynamically unstable intermediates as barriers in multi-electron redox reactions. *Aquatic Geochemistry*, *16*(3), 395–420. https://doi.org/10.1007/s10498-009-9082-3

Luther, G. W. (2023). Review on the physical chemistry of iodine transformations in the oceans. *Frontiers in Marine Science*, *10*. https://doi.org/10.3389/fmars.2023.1085618

Luther, G. W., & Campbell, T. (1991). Iodine speciation in the water column of the Black Sea. *Deep-Sea Research, Part A: Oceanographic Research Papers*, *38*, S875–S882. https://doi.org/10.1016/S0198-0149(10)80014-7

Luther, G. W., Findlay, A. J., MacDonald, D. J., Owings, S. M., Hanson, T. E., Beinart, R. A., & Girguis, P. R. (2011). Thermodynamics and kinetics of sulfide oxidation by oxygen: A look at inorganically controlled reactions and biologically mediated processes in the environment. *Frontiers in Microbiology*, *2*. https://doi.org/10.3389/fmicb.2011.00062

Luther, G. W., Swartz, C. B., & Ullman, W. J. (1988). Direct determination of iodide in seawater by cathodic stripping square wave voltammetry. *Analytical Chemistry*, *60*(17), 1721–1724. https://doi.org/10.1021/ac00168a017

Luther, G. W., Wu, J., & Cullen, J. B. (1995). Redox chemistry of iodine in seawater. In *Aquatic chemistry* (Vol. 244, pp. 135–155). American Chemical Society. https://doi.org/10.1021/ba-1995-0244.ch006

Margolskee, A., Frenzel, H., Emerson, S., & Deutsch, C. (2019). Ventilation pathways for the North Pacific oxygen deficient zone. *Global Biogeochemical Cycles*, *33*(7), 875–890. https://doi.org/10.1029/2018GB006149

McDougall, T. J., & Barker, P. M. (2011). *Getting started with TEOS-10 and the Gibbs Seawater (GSW) Oceanographic Toolbox*. SCOR/IAPSO WG127.

Moffett, J. W. (2024). Coupling of physical and chemical processes in the shelf to basin transport of iron and iodine off Washington and Oregon [Dataset]. Biological and Chemical Data Mangement Office. www.bco-dmo.org/project/889751

Moriyasu, R., Bolster, K. M., Hardisty, D. S., Kadko, D. C., Stephens, M. P., & Moffett, J. W. (2023). Meridional survey of the Central Pacific reveals iodide accumulation in equatorial surface waters and benthic sources in the abyssal plain. *Global Biogeochemical Cycles*, *37*(3), e2021GB007300. https://doi.org/10.1029/2021GB007300

Moriyasu, R., Evans, N., Bolster, K. M., Hardisty, D. S., & Moffett, J. W. (2020). The distribution and redox speciation of iodine in the eastern Tropical North Pacific Ocean. *Global Biogeochemical Cycles*, *34*(2), e2019GB006302. https://doi.org/10.1029/2019GB006302

Ohde, T., & Dadou, I. (2018). Seasonal and annual variability of coastal sulphur plumes in the northern Benguela upwelling system. *PLoS One*, *13*(2), e0192140. https://doi.org/10.1371/journal.pone.0192140

Peng, X., Fuchsman, C. A., Jayakumar, A., Oleynik, S., Martens-Habbena, W., Devol, A. H., & Ward, B. B. (2015). Ammonia and nitrite oxidation in the Eastern Tropical North Pacific. *Global Biogeochemical Cycles*, *29*(12), 2034–2049. https://doi.org/10.1002/2015GB005278

Podder, J., Lin, J., Sun, W., Botis, S. M., Tse, J., Chen, N., et al. (2017). Iodate in calcite and vaterite: Insights from synchrotron X-ray absorption spectroscopy and first-principles calculations. *Geochimica et Cosmochimica Acta*, *198*, 218–228. https://doi.org/10.1016/j.gca.2016.11.032

Python Software Foundation. (2022). Python language reference, 3.7.13 documentation. Retrieved from https://docs.python.org/release/3.7.13/

Raven, M. R., Keil, R. G., & Webb, S. M. (2020). Microbial sulfate reduction and organic sulfur formation in sinking marine particles. *Science*, *371*(6525), 178–181. https://doi.org/10.1126/science.abc6035

Raybaut, P. (2009). Spyder 5.1.5 documentation. https://www.spyder-ide.org/

Reyes-Umana, V., Henning, Z., Lee, K., Barnum, T. P., & Coates, J. D. (2021). Genetic and phylogenetic analysis of dissimilatory iodate-reducing bacteria identifies potential niches across the world's oceans. *The ISME Journal*, *16*, 1–12. https://doi.org/10.1038/s41396-021-01034-5

Rue, E. L., Smith, G. J., Cutter, G. A., & Bruland, K. W. (1997). The response of trace element redox couples to suboxic conditions in the water column. *Deep Sea Research Part I: Oceanographic Research Papers*, *44*(1), 113–134. https://doi.org/10.1016/S0967-0637(96)00088-X

Saunders, J. K., McIlvin, M. R., Dupont, C. L., Kaul, D., Moran, D. M., Horner, T., et al. (2022). Microbial functional diversity across biogeochemical provinces in the central Pacific Ocean. *Proceedings of the National Academy of Sciences*, *119*(37), e2200014119. https://doi.org/10.1073/pnas.2200014119

Scholz, F., Hardisty, D. S., & Dale, A. W. (2024). Early diagenetic controls on sedimentary iodine release and iodine-to-organic carbon ratios in the paleo-record. *Global Biogeochemical Cycles*, *38*(2), e2023GB007919. https://doi.org/10.1029/2023GB007919

Schunck, H., Lavik, G., Desai, D. K., Großkopf, T., Kalvelage, T., Löscher, C. R., et al. (2013). Giant hydrogen sulfide plume in the oxygen minimum zone off Peru supports chemolithoautotrophy. *PLoS One*, *8*(8), e68661. https://doi.org/10.1371/journal.pone.0068661

Severmann, S., McManus, J., Berelson, W. M., & Hammond, D. E. (2010). The continental shelf benthic iron flux and its isotope composition. *Geochimica et Cosmochimica Acta*, *74*(14), 3984–4004. https://doi.org/10.1016/j.gca.2010.04.022

Shaw, T. J., Luther, G. W., Rosas, R., Oldham, V. E., Coffey, N. R., Ferry, J. L., et al. (2021). Fe-catalyzed sulfide oxidation in hydrothermal plumes is a source of reactive oxygen species to the ocean. *Proceedings of the National Academy of Sciences of the United States of America*, *118*(40), e2026654118. https://doi.org/10.1073/pnas.2026654118

Siedlecki, S. A., Banas, N. S., Davis, K. A., Giddings, S., Hickey, B. M., MacCready, P., et al. (2015). Seasonal and interannual oxygen variability on the Washington and Oregon continental shelves. *Journal of Geophysical Research: Oceans*, *120*(2), 608–633. https://doi.org/10.1002/2014JC010254

Sperling, E. A., Wolock, C. J., Morgan, A. S., Gill, B. C., Kunzmann, M., Halverson, G. P., et al. (2015). Statistical analysis of iron geochemical data suggests limited late Proterozoic oxygenation. *Nature*, *523*(7561), 451–454. https://doi.org/10.1038/nature14589

Ştreangă, I.-M., Repeta, D. J., Blusztajn, J. S., & Horner, T. J. (2024). Speciation and cycling of iodine in the subtropical North Pacific Ocean. *Frontiers in Marine Science*, *10*. https://doi.org/10.3389/fmars.2023.1272968

The MathWorks, Inc. (2018). MATLAB release 2018b. Retrieved from https://www.mathworks.com/products/matlab.html

Thyng, K., Greene, C., Hetland, R., Zimmerle, H., & DiMarco, S. (2016). True colors of oceanography: Guidelines for effective and accurate colormap selection. *Oceanography*, *29*(3), 9–13. https://doi.org/10.5670/oceanog.2016.66

Tian, R. C., & Nicolas, E. (1995). Iodine speciation in the northwestern Mediterranean Sea, method and vertical profile. *Marine Chemistry*, *48*(2), 151–156. https://doi.org/10.1016/0304-4203(94)00048-I

Truesdale, V. W., & Bailey, G. W. (2000). Dissolved iodate and total iodine during an extreme hypoxic event in the Southern Benguela System. *Estuarine, Coastal and Shelf Science*, *50*(6), 751–760. https://doi.org/10.1006/ecss.2000.0609

Truesdale, V. W., & Upstill-Goddard, R. (2003). Dissolved iodate and total iodine along the British east coast. *Estuarine, Coastal and Shelf Science*, *56*(2), 261–270. https://doi.org/10.1016/S0272-7714(02)00161-0

Wadley, M. R., Stevens, D. P., Jickells, T. D., Hughes, C., Chance, R., Hepach, H., et al. (2020). A global model for iodine speciation in the upper ocean. *Global Biogeochemical Cycles*, *34*(9), e2019GB006467. https://doi.org/10.1029/2019GB006467

Winkelbauer, H., Cordova-Rodriguez, K., Reyes-Macaya, D., Scott, J., Glock, N., Lu, Z., et al. (2021). Foraminifera iodine to calcium ratios: Approach and cleaning. *Geochemistry, Geophysics, Geosystems*, *22*(11), e2021GC009811. https://doi.org/10.1029/2021GC009811

Wong, G. T. F., & Brewer, P. G. (1977). The marine chemistry of iodine in anoxic basins. *Geochimica et Cosmochimica Acta*, *41*(1), 151–159. https://doi.org/10.1016/0016-7037(77)90195-8

Zakem, E. J., & Follows, M. J. (2017). A theoretical basis for a nanomolar critical oxygen concentration. *Limnology & Oceanography*, *62*(2), 795–805. https://doi.org/10.1002/lno.10461